Theory of high-power excitation spectra of rf-SQUID

Olesia Dmytruk[●], R. H. Rodriguez[●], Ç. Ö. Girit[●], and Marco Schiró

JEIP, USR 3573 CNRS, Collège de France, PSL Research University, F-75321 Paris, France

We discuss the theory of linear and nonlinear spectroscopy of an rf superconducting quantum interference device (rf-SQUID) coupled to a Josephson spectrometer. Recent experimental measurements on this system have shown a strongly nonlinear absorption line shape, whose current peak maximum undergoes a forward-backward bending transition depending on the value of the rf-SQUID phase. We show that this transition can be qualitatively understood by mapping the dynamics of the driven rf-SQUID onto a generalized Duffing oscillator, with tunable drive and nonlinearity, undergoing a bifurcation. Finally we show that in order to quantitatively reproduce the experimental data reported by Griesmar *et al.* [Phys. Rev. Research **3**, 043078 (2021)], it is crucial to include the feedback from the load line, leading to an additional source of nonlinearity.

I. INTRODUCTION

Electrical devices based on Josephson junctions have been at the center of research attention for many years. Such devices are very versatile, as they can be used as qubits [1–8], metamaterials [9], Josephson bifurcation amplifiers [10–12], or detectors of mesoscopic systems [13–20]. Moreover, Josephson junctions with external time-dependent driving are suitable platforms for studying nonlinear phenomena [21–26].

The absorption spectroscopy of Josephson junctions is a powerful experimental technique that can be used to study mesoscopic systems in a wide frequency range [19,27]. Very recently, a novel Josephson junction spectrometer with a broad bandwidth and variable coupling strength was implemented and used to perform high-power spectroscopy on an rf superconducting quantum interference device (rf-SQUID) [28]. The current-voltage characteristic of the spectrometer, related to the absorption spectrum, was found to depend strongly on the phase of the rf-SQUID, φ_x. In particular the position of the current maximum was found to shift towards higher or lower frequencies depending on φ_x, resulting in a forward or backward bending of the absorption peak [28].

Motivated by this experiment, in this paper we present an effective model for an rf-SQUID strongly driven by the Josephson junction spectrometer and discuss its linear and nonlinear spectroscopy. The rf-SQUID consists of a single Josephson junction in a superconducting loop enclosing a magnetic flux Φ_x and it is inductively coupled to the spectrometer, which is formed by two Josephson junctions in a superconducting loop threaded by a magnetic flux Φ_s (see Fig. 1). In our effective model this inductive coupling results in a periodic driving of the rf-SQUID at a frequency set by the biasing voltage and amplitude controlled by Φ_s. We map the dynamics of the driven rf-SQUID in the semiclassical regime onto a generalized Duffing oscillator with tunable parameters.

In particular, we show that the sign of the leading Duffing nonlinearity can be tuned by changing the phase of the rf-SQUID, resulting in a forward-backward bending transition of the absorption spectrum. While capturing the qualitative features of the experiment, the mapping to the Duffing oscillator cannot by itself reproduce the observed line shape, which features a strong asymmetry between backward and forward bending. We show that accounting for the feedback from the load line, another key feature of the setup of Ref. [28], leads to an additional and sizable source of nonlinearity which is crucial to quantitatively reproduce the experimental results.

II. EFFECTIVE MODEL FOR rf-SQUID COUPLED TO A SPECTROMETER

To model the setup in Fig. 1 we consider an rf-SQUID whose Hamiltonian reads [2]

$$H_{\text{rf}} = E_C \hat{N}^2 + E_L[\hat{\varphi} - \varphi_x]^2 - E_J \cos(\hat{\varphi}). \tag{1}$$

Here, the first term describes the charging energy $E_C = 2e^2/C$, with C the capacitance of the junction and $\hat{N}$ the number of Cooper pairs conjugated to the phase $\hat{\varphi}$, $[\hat{N}, \hat{\varphi}] = -i$, while the second term accounts for the inductive energy $E_L = \varphi_0^2/(2L)$, with L the self-inductance of the loop, $\varphi_x = \Phi_x/\varphi_0$ the phase of the rf-SQUID, Φ_x the magnetic flux threading the loop, and $\varphi_0 = \Phi_0/(2\pi)$ the reduced flux quantum. Finally, the last term in Eq. (1) describes the Josephson nonlinearity of strength $E_J = I_0 \varphi_0$, with I_0 the critical current.

A microscopic model of the coupling between the rf-SQUID and spectrometer, including the basic quantum degrees of freedom of the latter, is discussed in detail in the Supplemental Material [29]. Here, we present an effective description according to which the inductive coupling between the rf-SQUID and spectrometer leads to an explicit periodic driving for the former at the Josephson frequency
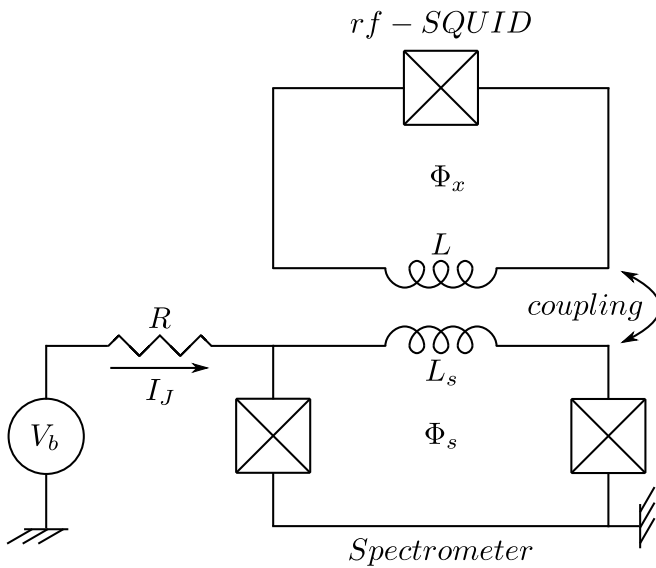
FIG. 1. Scheme of the setup: An rf-SQUID (top) coupled inductively to a Josephson junction spectrometer (bottom). The rf-SQUID is formed by a superconducting loop, threaded by a magnetic flux Φ_x, of inductance L with a single Josephson junction (boxed cross). The Josephson spectrometer consists of two voltage-biased Josephson junctions (boxed crosses) in a superconducting loop of inductance L_s enclosing a static magnetic flux Φ_s. A bias circuit with a voltage source V_b and resistor R supplies dc current I_J.

$\omega_J = 2eV_J/\hbar$, i.e.,

$$H_{\text{coupl}} = -2E_L A(\varphi_s) \cos(\omega_J t)\hat{\varphi}, \qquad (2)$$

where $A(\varphi_s) = kI_{0s}\varphi_0\sqrt{L_s/L}/(2E_L)\sin(\varphi_s/2)$ and V_J is the DC voltage across the spectrometer due to the source V_b. Here, k is the coupling coefficient between two inductive loops resulting from their mutual inductance, L_s is the inductance of the spectrometer loop, $\varphi_s = \Phi_s/\varphi_0$ is the phase difference across the spectrometer, with Φ_s being the magnetic flux through the spectrometer loop.

In order to include the dissipation, we couple the rf-SQUID to the bosonic bath, $H_{\text{bath}} = \sum_\alpha \hbar\omega_\alpha \hat{b}_\alpha^\dagger \hat{b}_\alpha$, such that we get

$$H = H_{\text{rf}} + H_{\text{coupl}} + H_{\text{bath}} + \hat{\varphi}\sum_\alpha g_\alpha(\hat{b}_\alpha + \hat{b}_\alpha^\dagger), \qquad (3)$$

where $\hat{b}_\alpha^\dagger$ ($\hat{b}_\alpha$) are bosonic creation (annihilation) operators of the bath, ω_α is the frequency of the bosonic bath, g_α is the coupling strength between the bosonic bath and rf-SQUID, and we assume an Ohmic spectral function for the bath.

III. SEMICLASSICAL DYNAMICS OF DRIVEN-DISSIPATIVE rf-SQUID

In this paper we focus on the regime $E_L \gg E_J \gg E_C$, which is relevant for the setup of Ref. [28]. For $E_J \gg E_C$ the flux $\hat{\varphi}$ is the quantum degree of freedom [2]. Therefore, we define [27] $\hat{\varphi} = \sqrt{2}\kappa\hat{X}$ and $\hat{N} = \hat{P}/(\sqrt{2}\kappa)$, where $\hat{X}, \hat{P}$ are harmonic oscillator variables, related to the bosonic creation (annihilation) operators of the plasma mode of the rf-SQUID, and κ is a dimensionless parameter given by $\kappa^2 = \sqrt{E_C/E_L}/2$.

The tunneling of Cooper pairs in the spectrometer is associated with the absorption of photons by the rf-SQUID [28]. Therefore, the resulting dc current I_J flowing in the spectrometer is proportional to the photon absorption rate Λ, $I_J = 2e\Lambda$. Treating the coupling Hamiltonian Eq. (2) as a time-dependent perturbation to an unperturbed Hamiltonian Eq. (1), Λ can be calculated using the Fermi's golden rule [29]

$$\Lambda = \frac{2\pi}{\hbar}[2E_L A(\varphi_s)]^2 2\kappa^2 |\langle i|\hat{X}|f\rangle|^2 \rho(E_f), \qquad (4)$$

where $\langle i|\hat{X}|f\rangle$ is the matrix element calculated between the initial and final states of H_{rf}, and $\rho(E_f)$ is the density of states at the energy E_f of the final states.

However, in the absence of the dissipation, the photon absorption rate will have delta peaks when the excitation energies of H_{rf} are in resonance with ω_J. To include bath degrees of freedom in our treatment, we formulate the problem in terms of the Keldysh action [30] and derive the semiclassical equation of motion for the classical coordinate X_{cl} [29]. Introducing a new variable $\tilde{X}_{\text{cl}}(t) = X_{\text{cl}}(t) - \varphi_x/\kappa$, the equation of motion for the classical field $\tilde{X}_{\text{cl}}(t)$ reads

$$\ddot{\tilde{X}}_{\text{cl}}(\tau) + \frac{\gamma}{\hbar}\dot{\tilde{X}}_{\text{cl}}(t) + \tilde{X}_{\text{cl}}(t) + 2\kappa\frac{E_J}{\hbar\omega_p}\sin[\kappa\tilde{X}_{\text{cl}}(\tau) + \varphi_x]$$
$$= \frac{A(\varphi_s)}{\kappa}\cos\left(\frac{\omega_J}{\omega_p}\tau\right), \qquad (5)$$

where γ is the dissipation, $\tau = t\omega_p$ is a dimensionless time, and $\omega_p = 1/\sqrt{LC}$. We note that Eq. (5) is similar to the resistively shunted junction (RSJ) model [31] but it allows us to include the microscopic details of the system. Moreover, the equation of motion derived using the Keldysh technique can be generalized to more complicated situations, such as the quantum regime, or a different form of dissipation. Expanding $\sin[\kappa\tilde{X}_{\text{cl}}(\tau)]$ up to third order in $\kappa \ll 1$, Eq. (5) takes the form of a *generalized Duffing equation*,

$$\ddot{\tilde{X}}_{\text{cl}}(\tau) + \frac{\gamma}{\hbar}\dot{\tilde{X}}_{\text{cl}}(\tau) + \Omega(\varphi_x)\tilde{X}_{\text{cl}}(\tau) + \frac{\partial V_{\text{nl}}}{\partial\tilde{X}_{\text{cl}}} = f(\tau), \qquad (6)$$

where $\Omega(\varphi_x)$ is the renormalized plasma frequency given by

$$\Omega(\varphi_x) = \omega_p\sqrt{1 + \beta_L\cos(\varphi_x)}, \qquad (7)$$

with $\beta_L = E_J/(2E_L)$, while V_{nl} accounts for the nonlinearity arising from the Josephson energy,

$$V_{\text{nl}} = \lambda(\varphi_x)\tilde{X}_{\text{cl}}^3(\tau) + \lambda'(\varphi_x)\tilde{X}_{\text{cl}}^4(\tau).$$

We note that the shape of the nonlinear potential is fully tunable by φ_x, since we have $\lambda(\varphi_x) = -\kappa^3 E_J \sin(\varphi_x)/(3\hbar\omega_p)$ and $\lambda'(\varphi_x) = -\kappa^4 E_J \cos(\varphi_x)/(12\hbar\omega_p)$. Finally, $f(\tau)$ in Eq. (6) is the time-dependent drive,

$$f(\tau) = -2\kappa\frac{E_J}{\hbar\omega_p}\sin(\varphi_x) + \frac{A(\varphi_s)}{\kappa}\cos\left(\frac{\omega_J}{\omega_p}\tau\right).$$

Equation (6) describes therefore a nonlinear differential equation in the presence of drive and dissipation, whose solution we will discuss in the following.

IV. FORWARD-BACKWARD TRANSITION IN THE NONLINEAR SPECTROSCOPY REGIME

Next, we calculate the average value of the coordinate $\langle X_{cl} \rangle$, obtained from the steady-state solution of Eq. (6), for different values of φ_x and φ_s. While a full numerical solution of the Duffing equation is reported for completeness in the Supplemental Material [29], here we discuss the results using a semianalytical approach that captures perfectly the features contained in the full numerics.

In the absence of any nonlinearity the solution of Eq. (6) takes the form

$$X_{cl}(t) = X_{cl}(\omega)\cos(\omega t + \phi), \tag{8}$$

where the frequency response $X_{cl}(\omega)$ has a peak at the renormalized plasma frequency $\Omega(\varphi_x)$. In the presence of nonlinear terms an ansatz of this form does not solve the Duffing equation exactly, yet we can still obtain a closed equation for $X_{cl}(\omega)$ by disregarding higher-order harmonics [29]. Solving this equation for different values of φ_x and φ_s allows us to obtain the result plotted in Fig. 2, where we show the frequency response for two different values of $\varphi_x = 0, \pi$ considered in Ref. [28], and for different values of φ_s corresponding to the evolution from the linear to the nonlinear spectroscopy regime. We note that for all values of the parameters considered in Fig. 2 the frequency response $X_{cl}(\omega)$ is always a single-valued function of ω, therefore it is a stable solution of Eq. (6). We see that in the linear spectroscopy regime the frequency response displays a small peak centered around $\Omega(\varphi_x)$, and the shape of the peak does not change as φ_x is varied. However, upon increasing the strength of the drive, the response becomes strongly anharmonic with a peak which increases in size and becomes more and more distorted. In particular, we see that upon tuning φ_x from zero to π the frequency response shows a transition from backward to forward bending. This transition can be immediately understood by noticing that in general, the steady-state solution of the Duffing equation is sensitive to the sign of the coefficient in front of the cubic term. In our case this coefficient depends explicitly on the phase of the rf-SQUID and in particular changes sign at $\varphi_x = \pi/2$,

$$\lambda'(\varphi_x) = -\kappa^4 E_J \cos(\varphi_x)/(12\hbar\omega_p),$$

leading therefore to a transition in the shape of the frequency response. Quite interestingly, a qualitatively similar behavior was found in the experimental results of Ref. [28], in particular, in the nonlinear spectroscopy regime. We will go back later on this point to present a quantitative comparison with the experimental data.

V. ROLE OF FEEDBACK FROM THE LOAD LINE

The previous section has highlighted the role of the Duffing nonlinearity and its tunability with the phase φ_x at the origin of the forward-backward transition in the frequency response of the rf-SQUID. Here, we discuss another source of nonlinear behavior, that is at play in the experimental setting of Ref. [28], namely the fact that the voltage effectively biasing the spectrometer, V_J, is different from the applied voltage V_b due to the finite resistance R in series with the circuit, i.e., $V_J = V_b - RI_J$. In the experiment both the voltage V_J across
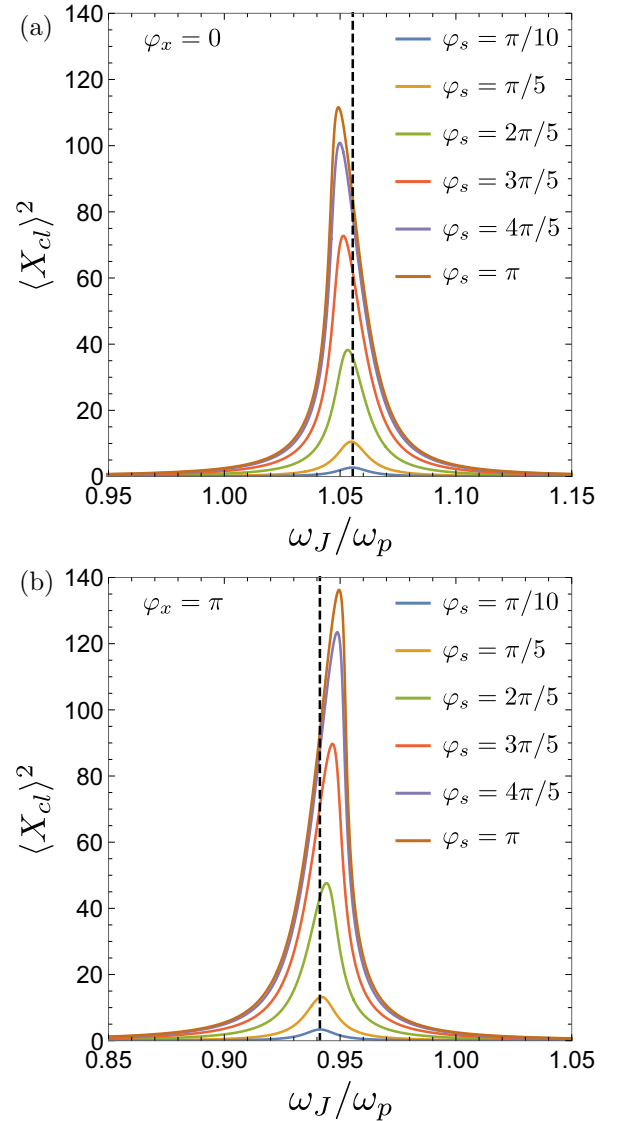

FIG. 2. Average value of the coordinate squared $\langle X_{cl} \rangle^2$ as a function of the frequency ω_J/ω_p for the phase of the rf-SQUID $\varphi_x = 0$ (top panel) and $\varphi_x = \pi$ (bottom panel). Different colors of the lines correspond to different values of φ_s, from bottom to top: $\varphi_s = \pi/10$, $\varphi_s = \pi/5$, $\varphi_s = 2\pi/5$, $\varphi_s = 3\pi/5$, $\varphi_s = 4\pi/5$, $\varphi_s = \pi$. The black dashed line corresponds to the frequency $\Omega(\varphi_x)$ given by Eq. (7). Both for (a) $\varphi_x = 0$ and (b) $\varphi_x = \pi$ the average value of the coordinate increases when increasing φ_s. (a) For $\varphi_x = 0$ the position of the peak in $\langle X_{cl} \rangle^2$ shifts to a smaller value of ω_J/ω_p, resulting in backward bending of $\langle X_{cl} \rangle^2$. (b) For $\varphi_x = \pi$ the position of the peak in $\langle X_{cl} \rangle^2$ shifts to a larger value of ω_J/ω_p, resulting in forward bending of the coordinate squared. Other parameters are fixed as $\omega_p = 2\pi \times 45, 91$ GHz, $\beta_L = E_J/(2E_L) = 0.114$, $L = 58$ pH, $L_S = 43.7$ pH, $I_{0s}/I_0 = 1/3$, $k = 0.5$, and $\gamma/\hbar = 0.017$.

the spectrometer and the current I_J flowing through it are independently measured, for different values of the applied voltage V_b. In order to fully account for this effect we would need to go beyond our effectively driven rf-SQUID model and include the dynamics of the spectrometer, which however goes beyond the scope of this work. Still, we can phenomenologically take into account the finite resistance $R \neq 0$ in the circuit in Fig. 1
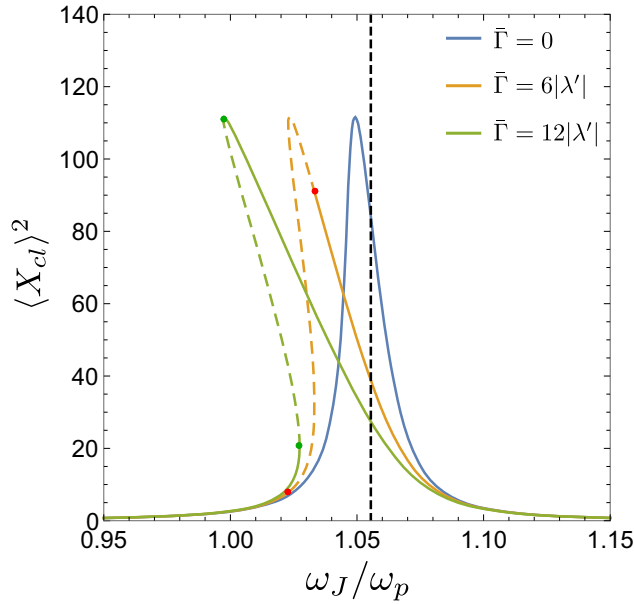
FIG. 3. Average value of the coordinate squared $\langle X_{cl}\rangle^2$ as a function of the driving frequency ω_J/ω_p in the presence of the feedback from the load line, leading to a drive frequency which depends on the value of the oscillator coordinate, see Eq. (9). The phase of the rf-SQUID is fixed to zero, $\varphi_x = 0$. The blue line corresponds to $\bar{\Gamma} = 0$, the orange line corresponds to $\bar{\Gamma} = 6|\lambda'(0)|$, and the green line corresponds to $\bar{\Gamma} = 12|\lambda'(0)|$. The dashed lines denote unstable solutions, and red (green) circles denote the solutions at the jump frequencies. The vertical black dashed line corresponds to the frequency $\Omega(\varphi_x)$ given by Eq. (7). Other parameters are the same as in Fig. 2.

by assuming that the frequency at which the Duffing oscillator is driven, i.e., ω_J in Eq. (5), depends self-consistently on the average value of the oscillator coordinate,

$$\omega_J \rightarrow \omega_J + \bar{\Gamma}\omega_p\langle X_{cl}\rangle^2, \tag{9}$$

where we used the relation $I_J = \Gamma\langle X_{cl}\rangle^2$. Here, $\bar{\Gamma} = 2eR\Gamma/(\hbar\omega_p)$. This feedback mechanism introduces an additional source of nonlinear behavior as we show in Fig. 3, where we plot the frequency response for $\varphi_x = 0$, for a fixed value of the Duffing nonlinearity, and different values of the feedback parameter $\bar{\Gamma}$. We see that the strength of the back bending becomes stronger and stronger upon increasing the feedback effect from the load line. Moreover, in the presence of the feedback, the frequency response $X_{cl}(\omega)$ becomes not a single-valued function of ω, therefore the solution is unstable. By setting the discriminant of the equation for X_{cl} to zero, we can find the jump-up and jump-down frequencies numerically, and the region between the jump-up and jump-down frequencies will correspond to the unstable solution [29]. We further notice that from the experimental parameters used in Ref. [28] we estimate that the feedback contribution to the voltage is sizable, of the order of $\delta V_J \sim 38~\mu$V for an averaged measured voltage $V_J \sim 96~\mu$V. In the next section, we are going to present a detailed quantitative comparison with the experimental results that show how both effects, namely tunable Duffing nonlinearity and feedback, are needed to reproduce the results.
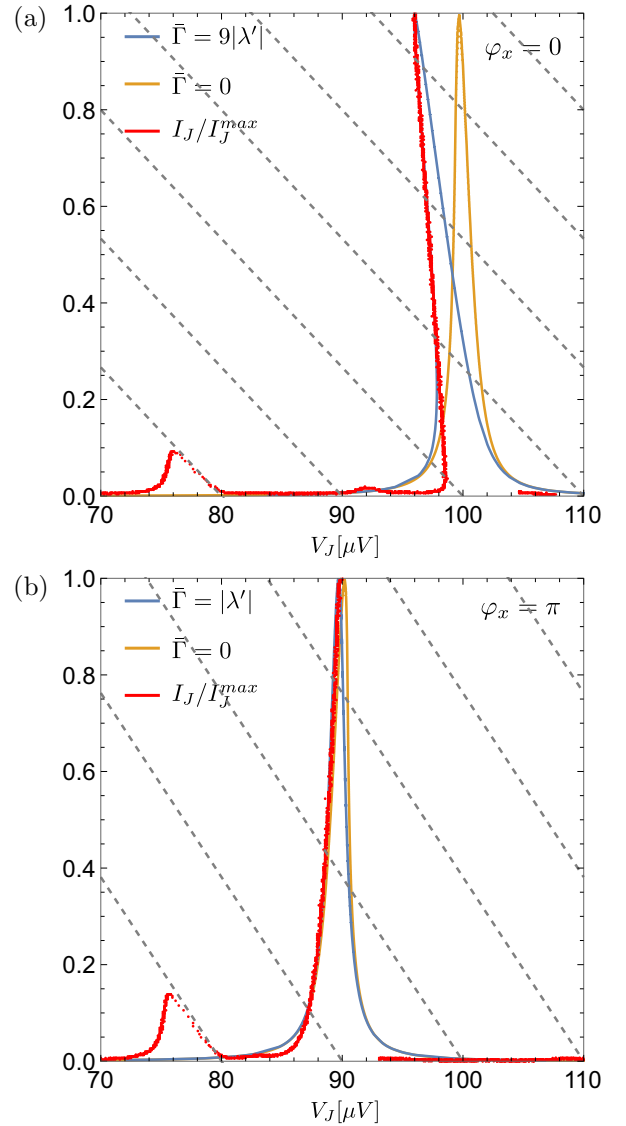

FIG. 4. Normalized average value of the coordinate squared $\langle X_{cl}\rangle^2/\langle X_{cl}\rangle^2_{max}$ as a function of bias voltage V_J (μV) for (a) $\varphi_x = 0$ and (b) $\varphi_x = \pi$. The orange line corresponds to $\langle X_{cl}\rangle^2/\langle X_{cl}\rangle^2_{max}$ calculated for the constant voltage $V_J \equiv V_b$ (in the absence of the feedback). The blue line corresponds to $\langle X_{cl}\rangle^2/\langle X_{cl}\rangle^2_{max}$ calculated in the presence of the feedback on the applied voltage, $V_J = V_b - R\Gamma\langle X_{cl}\rangle^2$, see Eq. (9). The experimental data for the current (divided by its maximum value) are presented by red dots. A good agreement between I_J/I_J^{max} and $\langle X_{cl}\rangle^2/\langle X_{cl}\rangle^2_{max}$ (calculated in the presence of the feedback) can be achieved by tuning $\bar{\Gamma} = 9|\lambda'(0)|$ (top) or $\bar{\Gamma} = |\lambda'(\pi)|$ (bottom). Gray dashed lines are given by the function $I_J/I_J^{max} = (V_b - V_J)/(RI_J^{max})$ plotted for several values of bias voltage V_b and correspond to the current obtained in experimental measurements [28]. Other parameters are the same as in Fig. 2.

VI. COMPARISON WITH EXPERIMENTAL DATA

We conclude by comparing the prediction of our theory for the frequency response of the rf-SQUID with the experimental data obtained through the Josephson spectrometer. We focus again on two specific values of the rf-SQUID phase, $\varphi_x = 0, \pi$ showing respectively backward and forward bending and fix

the phase of the spectrometer to $\varphi_s = \pi$, namely the strong drive regime. We note that there are two free parameters in the model, γ and Γ, that are not fixed by the measurements [28]. We emphasize that our theory mainly focuses on the backward/forward bending transition rather than on the peak height of the current measured in the experiment, therefore we compare theoretical and experimental data normalized by their maximum value. Let us first consider the case of $\varphi_x = 0$. The current-voltage characteristic (normalized by its maximum value) is presented in Fig. 4 (red line). In the same figure, we plot the average value of the coordinate squared (normalized by its maximum value) in the absence of the feedback, $\bar{\Gamma} = 0$ (orange line). We note that the position of the maximum in the current-voltage characteristic in V_J is smaller than the position of the maximum in $\langle X_{cl} \rangle^2$. Therefore, I_J bends stronger than $\langle X_{cl} \rangle^2$ in the absence of the feedback. To find a better agreement between the experimental data and theoretical predictions, we include a feedback effect in the calculation of $\langle X_{cl} \rangle^2$. As expected, the finite $\bar{\Gamma}$ increases the bending of $\langle X_{cl} \rangle^2$ as a function of the bias V_J [see Fig. 4(a) (blue line)]. Moreover, by choosing a specific value of $\bar{\Gamma}$ we can find a good agreement between the experimental data for the current I_J and calculated $\langle X_{cl} \rangle^2$ in the limit of a large number of photons (semiclassical approximation). Similarly, for the case $\varphi_x = \pi$, we see that our theory is able to capture the forward bending but in order to quantitatively reproduce the data the inclusion of the feedback mechanism is important. Furthermore, we note that the agreement with the experimental data is excellent for large values of the current, corresponding to large photon numbers, as expected for our semiclassical theory, while at low intensity quantum fluctuations are likely crucial to capture the sharp edge seen in the current-voltage characteristic. Finally, we note that only one branch of the current-voltage characteristic can be accessed experimentally, as it appears clearly from Fig. 4. We can qualitatively understand the origin of this effect by comparing on the same plot the theoretical data for $\langle X_{cl} \rangle^2 / \langle X_{cl} \rangle^2_{max}$ with

the lines $I_J / I_J^{max} = (V_b - V_J)/(R I_J^{max})$ corresponding to the current obtained in experimental measurements [28]. From this comparison we can see that in fact only the left branch of the curve is accessible. We emphasize however that a full microscopic theory for the current-voltage characteristic through the spectrometer, able to capture the maximum current height as well as its region of in-stability, will necessary need to go beyond our driven rf-SQUID effective model and it is left for future studies.

VII. CONCLUSIONS

We studied an rf-SQUID inductively coupled to the spectrometer based on two Josephson junctions. We calculated the average value of the phase difference across the rf-SQUID, which is proportional to the current flowing in the spectrometer, and found that the position of the peak in the frequency response is given by $\Omega(\varphi_x)$ and, therefore, depends on the rf-SQUID phase φ_x. For large values of φ_s, corresponding to the nonlinear spectroscopy regime, we found that the peak maximum shifts to higher (lower) values of the frequency for $\varphi_x > \pi/2$ ($\varphi_x < \pi/2$), leading to the forward (backward) bending of the peak. Moreover, taking into account the feedback from the load line allows us to get a quantitative agreement with the experimental data [28].

ACKNOWLEDGMENTS

[1] Y. Makhlin, G. Schön, and A. Shnirman, Josephson-junction qubits with controlled couplings, Nature (London) **398**, 305 (1999).

[2] Y. Makhlin, G. Schön, and A. Shnirman, Quantum-state engineering with Josephson-junction devices, Rev. Mod. Phys. **73**, 357 (2001).

[3] D. Vion, A. Aassime, A. Cottet, P. Joyez, H. Pothier, C. Urbina, D. Esteve, and M. H. Devoret, Manipulating the quantum state of an electrical circuit, Science **296**, 886 (2002).

[4] A. Wallraff, D. I. Schuster, A. Blais, L. Frunzio, R.-S. Huang, J. Majer, S. Kumar, S. M. Girvin, and R. J. Schoelkopf, Strong coupling of a single photon to a superconducting qubit using circuit quantum electrodynamics, Nature (London) **431**, 162 (2004).

[5] G. Wendin and V. Shumeiko, Quantum bits with Josephson junctions, Low Temp. Phys. **33**, 724 (2007).

[6] T. D. Ladd, F. Jelezko, R. Laflamme, Y. Nakamura, C. Monroe, and J. L. O'Brien, Quantum computers, Nature (London) **464**, 45 (2010).

[7] I. Buluta, S. Ashhab, and F. Nori, Natural and artificial atoms for quantum computation, Rep. Prog. Phys. **74**, 104401 (2011).

[8] G. Wendin, Quantum information processing with superconducting circuits: A review, Rep. Prog. Phys. **80**, 106001 (2017).

[9] P. Jung, S. Butz, M. Marthaler, M. V. Fistul, J. Leppäkangas, V. P. Koshelets, and A. V. Ustinov, Multistability and switching in a superconducting metamaterial, Nat. Commun. **5**, 3730 (2014).

[10] I. Siddiqi, R. Vijay, F. Pierre, C. M. Wilson, M. Metcalfe, C. Rigetti, L. Frunzio, and M. H. Devoret, rf-Driven Josephson Bifurcation Amplifier for Quantum Measurement, Phys. Rev. Lett. **93**, 207002 (2004).

[11] I. Siddiqi, R. Vijay, F. Pierre, C. M. Wilson, L. Frunzio, M. Metcalfe, C. Rigetti, R. J. Schoelkopf, M. H. Devoret, D. Vion, and D. Esteve, Direct Observation of Dynamical Bifurcation between Two Driven Oscillation States of a Josephson Junction, Phys. Rev. Lett. **94**, 027005 (2005).

[12] S. Boutin, P. L. Lopes, A. Mu, U. C. Mendes, and I. Garate, Topological Josephson bifurcation amplifier: Semiclassical theory, J. Appl. Phys. **129**, 214302 (2021).

[13] J. Edstam and H. Olsson, Josephson broadband spectroscopy to 1 THz, Appl. Phys. Lett. **64**, 2733 (1994).

[14] T. Holst, D. Esteve, C. Urbina, and M. H. Devoret, Effect of a Transmission Line Resonator on a Small Capacitance Tunnel Junction, Phys. Rev. Lett. **73**, 3455 (1994).

[15] R. Lindell, J. Penttilä, M. Sillanpää, and P. Hakonen, Quantum states of a mesoscopic SQUID measured using a small Josephson junction, Phys. Rev. B **68**, 052506 (2003).

[16] P.-M. Billangeon, F. Pierre, H. Bouchiat, and R. Deblock, Very High Frequency Spectroscopy and Tuning of a Single-Cooper-Pair Transistor with an On-Chip Generator, Phys. Rev. Lett. **98**, 126802 (2007).

[17] I. Petković, M. Aprili, S. E. Barnes, F. Beuneu, and S. Maekawa, Direct dynamical coupling of spin modes and singlet Josephson supercurrent in ferromagnetic Josephson junctions, Phys. Rev. B **80**, 220502(R) (2009).

[18] J. Basset, H. Bouchiat, and R. Deblock, High-frequency quantum admittance and noise measurement with an on-chip resonant circuit, Phys. Rev. B **85**, 085435 (2012).

[19] L. Bretheau, Ç. Girit, H. Pothier, D. Esteve, and C. Urbina, Exciting Andreev pairs in a superconducting atomic contact, Nature (London) **499**, 312 (2013).

[20] D. J. Van Woerkom, A. Proutski, B. Van Heck, D. Bouman, J. I. Väyrynen, L. I. Glazman, P. Krogstrup, J. Nygård, L. P. Kouwenhoven, and A. Geresdi, Microwave spectroscopy of spinful Andreev bound states in ballistic semiconductor Josephson junctions, Nat. Phys. **13**, 876 (2017).

[21] M. Dykman, *Fluctuating Non-Linear Oscillators: From Nanomechanics to Quantum Superconducting Circuits* (Oxford University Press, Oxford, U.K., 2012).

[22] V. E. Manucharyan, E. Boaknin, M. Metcalfe, R. Vijay, I. Siddiqi, and M. Devoret, Microwave bifurcation of a Josephson junction: Embedding-circuit requirements, Phys. Rev. B **76**, 014524 (2007).

[23] A. B. Zorin and Y. Makhlin, Period-doubling bifurcation readout for a Josephson qubit, Phys. Rev. B **83**, 224506 (2011).

[24] D. P. DiVincenzo and J. A. Smolin, Nonlinear spectroscopy of superconducting anharmonic resonators, New J. Phys. **14**, 013051 (2012).

[25] J. Gosner, B. Kubala, and J. Ankerhold, Quantum properties of a strongly driven Josephson junction, Phys. Rev. B **99**, 144524 (2019).

[26] B. Lang and A. D. Armour, Multi-photon resonances in Josephson junction-cavity circuits, New J. Phys. **23**, 033021 (2021).

[27] L. Bretheau, Ç. Ö. Girit, M. Houzet, H. Pothier, D. Esteve, and C. Urbina, Theory of microwave spectroscopy of Andreev bound states with a Josephson junction, Phys. Rev. B **90**, 134506 (2014).

[28] J. Griesmar, R. H. Rodriguez, V. Benzoni, J.-D. Pillet, J.-L. Smirr, F. Lafont, and Ç. Ö. Girit, Superconducting on-chip spectrometer for mesoscopic quantum systems, Phys. Rev. Research **3**, 043078 (2021).

[29] See Supplemental Material at http://link.aps.org/supplemental/10.1103/PhysRevB.104.214508 for the derivation of the microscopic Hamiltonian starting from the full circuit.

[30] A. Kamenev, *Field Theory of Non-Equilibrium Systems* (Cambridge University Press, Cambridge, U.K., 2011).

[31] K. K. Likharev, *Dynamics of Josephson Junctions and Circuits* (Gordon and Breach, London, 1986).